Vertical subwavelength mode confinement in terahertz and mid-infrared quantum cascade lasers

E. Strupiechonski,[1] D. Grassani,[1] D. Fowler,[1] F. H. Julien,[1] S. P. Khanna,[2] L. Li,[2] E. H. Linfield,[2] A. G. Davies,[2] A. B. Krysa,[3] and R. Colombelli[1,a)]
[1]*Institut d'Electronique Fondamentale, UMR8622 CNRS, Univ. Paris Sud, 91405 Orsay, France*
[2]*School of Electronic and Electrical Engineering, University of Leeds, Leeds LS2 9JT, United Kingdom*
[3]*Department of Electronic and Electrical Engineering, EPSRC National Centre for III-V Technologies, University of Sheffield, Sheffield S1 3JD, United Kingdom*

(Received 22 September 2010; accepted 10 February 2011; published online 7 March 2011)

We exploit the modal confinement properties of metal-metal ridge waveguides to investigate the effect of reducing the thickness of the active laser cores in both terahertz and mid-infrared quantum cascade lasers. Devices with active regions over 55 times thinner than the free-space emission wavelength are demonstrated. They show only a modest increase in threshold current density compared with conventional-thickness devices. The limited increase in threshold is possibly due to a parasitic current channel in addition to the radiative current channel. These structures could be useful for the development of ultra-low volume lasers. © *2011 American Institute of Physics*. [doi:10.1063/1.3560980]

By exploiting the quantum mechanical properties of confined electrons, quantum cascade laser (QCL) technology provides a means of producing compact, electrically pumped semiconductor sources of coherent radiation in both the mid-infrared and terahertz (THz) spectral ranges of the electromagnetic spectrum. Unlike conventional bipolar semiconductor lasers, the emission wavelength, λ, can be precisely engineered *through* the composition and design of the heterostructure layer sequence.[1] QCL devices typically contain laser active regions (ARs) that are several microns thick and comprise several hundred nanometer-scale semiconductor layers of precisely controlled thicknesses and compositions. While representing a considerable achievement in heterostructure growth technology, this requirement is challenging and presents a significant barrier to the commercial implementation of QCL technology.

In order to confine the light vertically in mid-IR QCLs, semiconductor cladding layers are typically used to form dielectric optical waveguides, taking advantage of the refractive index contrast.[2] As with the subsequent single surface plasmon designs,[3] these waveguides require that the AR thickness, t_{AR} is greater than the free-space wavelength, λ, to ensure a suitably high mode confinement, Γ. In contrast, the metal-metal waveguides,[4] which use the surface plasmon polariton modes existing at the interface of the semiconductor AR with upper and lower metal layers, ensure Γ approaches 100% regardless of t_{AR}. This almost complete vertical light confinement allows the investigation of waveguides with vertical subwavelength light confinement such that $t_{AR} < \lambda/n_{AR}$,[5,6] where n_{AR} is the effective index of the laser mode. This is critical for the ongoing "miniaturization" of optoelectronic components, e.g., photonic crystal lasers and nanolasers.[7,8]

In this letter, we study the behavior of QCLs as a function of AR thickness for both mid-IR (at $\lambda \approx 15.5$ μm) and THz (at $\lambda \approx 96$ μm) devices employing metal-metal waveguides. We show that in both spectral regions the almost complete vertical light confinement provided by a metal-metal waveguide permits a significant reduction in the AR thickness while incurring—for THz devices—only a relatively small penalty in terms of increased laser threshold current density, J_{th} (smaller than what simple waveguide loss calculations predict). Our study shows how the device behavior is affected by the introduction of strong vertical subwavelength light confinement, and at the same time demonstrates the possibility of significantly reducing the length of time required for the growth of QCLs.

For measurements in the THz spectral range, three GaAs–$Al_{0.15}Ga_{0.85}As$ $\lambda = 96$ μm QCLs with 'resonant-phonon' AR designs were grown by molecular beam epitaxy with $t_{AR} = 10, 5, 2.5$ μm (samples L421, L420, and L422, respectively); the layer structure is given in Ref. 9. To improve electrical injection, Si-doped (2×10^{18} cm^{-3}) GaAs contact layers 75 nm and 50 nm thick were grown above and below the AR, respectively. After thermo-compressive gold-gold wafer bonding to carrier GaAs substrates and substrate removal with a selective etch based on citric acid, wet chemical etching (using a 1:8:120 H_2SO_4:H_2O_2:H_2O solution) of the $t_{AR} = 2.5$ μm wafer provided two further samples with $t_{AR} = 2$ and 1.75 μm, *albeit* sacrificing the 50 nm doped contact layer. Note that the thinnest device is over 55 times thinner than the free-space emission wavelength. All the THz devices were processed into Fabry–Pérot ridges, 90 to 220 μm wide, and cleaved into lengths between 1 and 2 mm. Non-annealed top Ti/Au contacts were used.

For the mid-IR devices, a $\lambda \approx 15.5$ μm, 4.25-μm-thick QCL with a "bound to continuum" AR design was grown by metal-organic vapor phase epitaxy using the $In_{0.53}Ga_{0.47}As/Al_{0.48}In_{0.52}As$ material system on an InP substrate with the layer structure given in Ref. 10. InGaAs contact facilitating layers, Si-doped at 2×10^{18} cm^{-3}, of 50 nm and 200 nm thicknesses were grown above and below the AR, respectively. After wafer bonding, a series of samples with $t_{AR} = 3.1$, 2.1, 1.1, and 0.75 μm were produced using the same slow wet etching technique described above, starting from the original $t_{AR} = 4.25$ μm sample. All the mid-IR

a)Electronic mail: raffaele.colombelli@u-psud.fr.

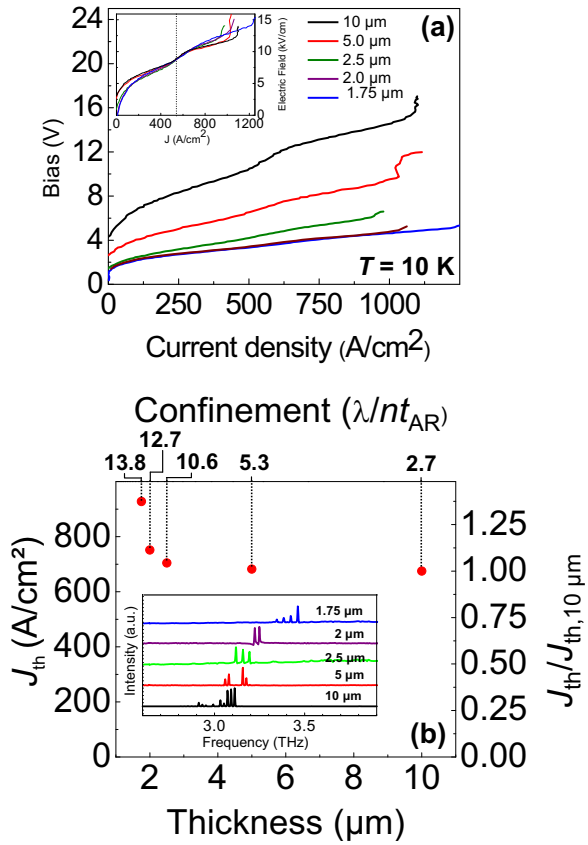

FIG. 1. (Color online) (a) Voltage-current density characteristics measured at a temperature of 10 K for $\lambda=96$ μm laser devices with different AR thicknesses. Inset: corrected electric field-current density curves. (b) Threshold current density as a function of AR thickness at $T=10$ K. Inset: pulsed (1% duty cycle) emission spectra for all t_{AR}. The spectra were measured in rapid scan mode using a Bruker Fourier transform infrared spectrometer and a liquid-He cooled Si-bolometer. The spectral resolution is 0.125 cm^{-1}.

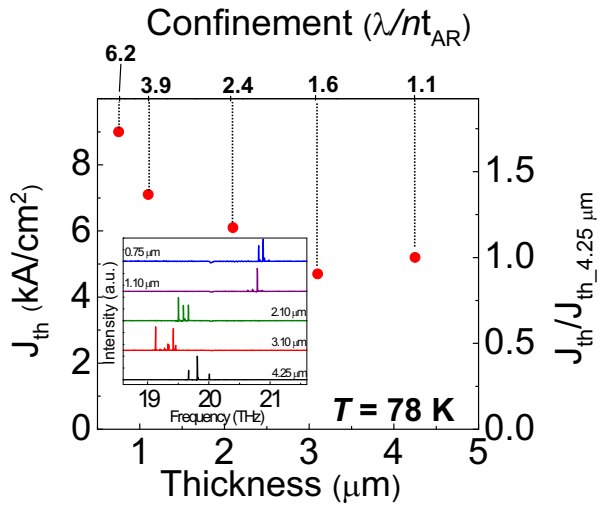

FIG. 2. (Color online) Threshold current density as a function of AR thickness at $T=78$ K for $\lambda=15.5$ μm laser devices. Inset: pulsed (1% duty cycle) emission spectra for all t_{AR}. The spectra were measured in rapid scan using a Nicolet Fourier transform infrared spectrometer and a liquid-nitrogen HgCdTe detector. The spectral resolution is 0.125 cm^{-1}.

devices were then processed using standard techniques into 500×80 μm^2 Fabry–Pérot ridge waveguides with Ti/Au top contacts.

Both the THz and mid-IR lasers were indium soldered epilayer-side up onto copper mounts, wire bonded, and mounted into a cryostat for electrical and optical characterization.

Figure 1(a) shows voltage—current density, *V-J*, characteristics for the $\lambda\approx96$ μm devices. The variation in alignment bias due to the different electric field in devices with different thickness can be clearly seen. Indeed, after accounting for the cable resistance of 0.6 Ω and the different voltage offset in the 1.75 and 2 μm thinned samples owing to loss of the doped contact layer (experimentally estimated to be ~0.15 V) the inset in Fig. 1(a) shows that when J is plotted against the applied electric field, $E=V/t_{AR}$, the curves superpose. The increase in differential resistance at a current density ≈550 Acm^{-2} indicates the onset of bandstructure alignment. Its consistent position for all t_{AR} shows the equivalence of the AR in each device.

Figure 1(b) shows a plot of the threshold current density, J_{th}, as a function of t_{AR} for the $\lambda\approx96$ μm devices at $T=10$ K in pulsed operation with a duty cycle of 1%. Consistent with an earlier study,[6] J_{th} is almost unaffected by a reduction in t_{AR} by a factor of two from 10 μm ($J_{th\text{-}10\ \mu m}=675$ A/cm^2,[6]) to 5 μm ($J_{th\text{-}5\ \mu m}=682$ A/cm^2). Further reduction in t_{AR} leads to a more rapid increase in J_{th}. However, for $t_{AR}=1.75$ μm, where the confinement, C, defined as the *effective* wavelength divided by the AR thickness, $(\lambda/n_{AR})/t_{AR}=15.7$ ($\lambda/t_{AR}\approx55$), $J_{th}/J_{th\text{-}10\ \mu m}$ rises modestly to just 1.4 ($J_{th\text{-}1.75\ \mu m}=928$ A/cm^2), while the calculated waveguide losses are about 3.3 times greater than those at 10 μm. The Fig. 1(b) inset shows a monotonic increase in emission frequency from 3.1 THz ($\lambda\approx96$ μm) to 3.4 THz ($\lambda\approx88$ μm) between $t_{AR}=10$ μm and $t_{AR}=1.75$ μm. Since J_{th} and hence the threshold voltage, V_{th}, is larger for thinner ARs, the observed blueshift is consistent with the expected Stark shift owing to the lightly diagonal lasing transition in the THz "resonant-phonon" three quantum well AR design.[11]

Figure 2 shows J_{th} as a function of t_{AR} measured at $T=78$ K, for the $\lambda\approx15.5$ μm mid-IR devices. The thinnest device (0.75 μm), with $C=6.3$, showed a threshold current density ~1.8 times higher than the 4.25 μm ($C=1.1$) device. The slight reduction in J_{th} observed between the 4.25-μm-thick and 3.1-μm-thick devices may be due to the removal of the lossy 200-nm-thick, highly doped contact layer in the first stage of the AR thinning.

The Fig. 2 inset shows that the emission frequency generally increases as t_{AR} is reduced, from 19.4 THz ($\lambda=15.5$ μm) for the 4.25 μm sample to 21 THz ($\lambda=14.3$ μm) for the 0.75 μm sample, although a slightly higher than expected frequency is measured for the 3.1-μm-thick sample. This behavior is again generally consistent with the Stark shift expected for the diagonal radiative transition of the bound-to-continuum AR design and the higher V_{th} of thinner AR devices. These data show—as expected—that at mid-IR wavelengths the thickness reduction is obtained at the expense of a larger increase in J_{th} with respect to the THz. However, in this case too it is possible to obtain functional devices, albeit at cryogenic temperatures, with extremely subwavelength active core thicknesses.

In a laser, J_{th} is proportional to $(\alpha_{wg}+\alpha_m)/\Gamma G$, where α_{wg} and α_m are the waveguide and mirror losses, respectively, and G is the gain of the AR.[2] For both the mid-IR and THz devices studied, the band structure design and therefore

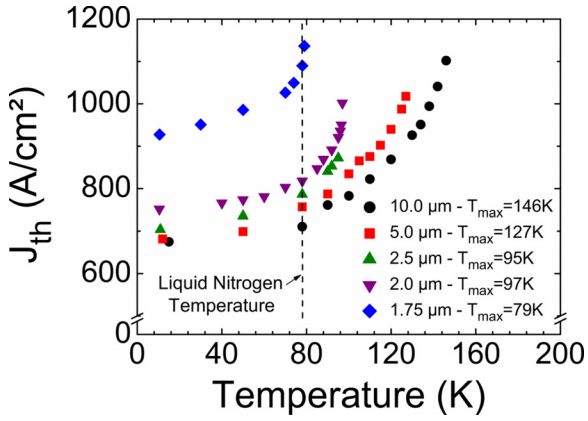

FIG. 3. (Color online) Threshold current density as a function of temperature for all the THz lasers with different AR thicknesses.

the gain remains, in principle, constant for all devices with different t_{AR}. The confinement factor Γ can be assumed to be almost 100% in all the metal-metal devices and to a first approximation we can assume $\alpha_{wg} \gg \alpha_m$. Thus, the observed increase in J_{th} with decreasing t_{AR} can be assumed to be due to the increase in α_{wg} as the AR thickness is reduced. This enhancement in the losses is expected due to the greater field intensity at the metal interface as the waveguide confinement is increased. This explanation is supported by the more rapid increase in J_{th} as a function of confinement observed in the mid-IR devices compared with the THz devices. At $\lambda \approx 96$ μm the behavior of gold is in fact much closer to that of a perfect metal than at $\lambda \approx 15.5$ μm (for gold: $n_{THz} = 239 + i \cdot 404$ whereas $n_{15.5\ \mu m} \sim 18.7 + i \cdot 112$).[12] This means that—at mid-IR frequencies—the calculated waveguide propagation losses are highly dependent on the chosen n,k values for gold, which are themselves strongly wavelength dependent in this spectral region. While this hinders a quantitative comparison with experimental data, such calculations showed clearly that the measured increase in J_{th} as the AR thickness is reduced—for both THz and mid-IR devices—was significantly less than the loss calculations would suggest. For instance, at $\lambda \approx 96$ μm $\alpha_{1.75\ \mu m}/\alpha_{10\ \mu m} \sim 3.3$, cf., $J_{th\text{-}1.75\ \mu m}/J_{th\text{-}10\ \mu m} = 1.4$; at $\lambda \approx 15.5$ μm $\alpha_{0.75\ \mu m}/\alpha_{4.25\ \mu m} \sim 5$, cf., $J_{th\text{-}0.75\ \mu m}/J_{th\text{-}4.25\ \mu m} = 1.8$ (calculations performed with the same indexes for gold as above).

The explanation for the observed disagreement between the computed losses and measured thresholds is possibly the existence—in THz QCLs—of a strong leakage current channel prior to alignment.[13,14] In this picture, the current density flowing in a QCL under operating conditions is the sum of the current responsible for the generation of photons, which traverses the intended path through the QCL band structure, and a leakage current which arises from unintended, conduction channels through the AR and which does not contribute to photon emission. Since only the current responsible for photon emission is proportional to the total losses, a large loss increase can lead to a modest J_{th} increase.

It should be mentioned that the thinner lasers have worse temperature performance as a consequence of the higher losses, as shown in Fig. 3. Finally, we observed—as expected because of the lower mirror losses—a progressive reduction in output laser power as the thickness of the AR was reduced. However, an accurate characterization of this effect will require integration of the output power across the entire laser far-field pattern, which is hard to quantify owing to the diffuse nature of the output beam from edge-emitting metal-metal waveguides.[15]

In conclusion, we have demonstrated that the strong vertical mode confinement in metal-metal waveguides allows the reduction in the thickness of both mid-IR and THz QCL ARs far below the effective wavelength without a large increase in J_{th} for THz devices. This result may considerably ease the demanding growth conditions for QCL ARs for which high power output is not a priority. Such thin QCL ARs have also potential applications in the development of microcavity lasers with extremely sub-wavelength effective volumes,[16] photonic crystal devices with reduced dimension,[17] and patch-cavity lasers.[18,19] Furthermore, adjusting the thickness of the same laser AR enables the study of the variation in device performance directly resulting from changing the waveguide losses.

The device fabrication has been performed at the nanocenter CTU-IEF-Minerve, partially funded by the "Conseil Général de l'Essonne." This work was supported by the French National Research Agency (Grant No. ANR-09-NANO-017 "Hi-Teq"), the RTRA project "LongWave," the European Research Council programmes "*NOTES*" and "*TOSCA*," and the EPSRC (UK) (Grant No. EP/E048811).

[1] *Intersubband Transitions in Quantum Structures*, edited by R. Paiella (McGraw-Hill, New York, 2006).
[2] C. Gmachl, F. Capasso, D. L. Sivco, and A. Y. Cho, Rep. Prog. Phys. **64**, 1533 (2001).
[3] R. Colombelli, F. Capasso, C. Gmachl, A. L. Hutchinson, D. L. Sivco, A. Tredicucci, M. C. Wanke, A. M. Sergent, and A. Y. Cho, Appl. Phys. Lett. **78**, 2620 (2001).
[4] K. Unterrainer, R. Colombelli, C. Gmachl, F. Capasso, H. Y. Hwang, A. M. Sergent, D. L. Sivco, and A. Y. Cho, Appl. Phys. Lett. **80**, 3060 (2002).
[5] B. S. Williams, S. Kumar, H. Callebaut, and Q. Hu, Appl. Phys. Lett. **83**, 2124 (2003).
[6] Y. Chassagneux, J. Palomo, R. Colombelli, S. Barbieri, S. Dhillon, C. Sirtori, H. Beere, J. Alton, and D. Ritchie, Electron. Lett. **43**, 285 (2007).
[7] S. Noda, Science **314**, 260 (2006).
[8] M. P. Nezhad, A. Simic, O. Bondarenko, B. Slutsky, A. Mizrahi, L. Feng, V. Lomakin, and Y. Fainman, Nat. Photonics **4**, 395 (2010).
[9] Y. Chassagneux, R. Colombelli, W. Maineult, S. Barbieri, S. P. Khanna, E. H. Linfield, and A. G. Davies, Opt. Express **17**, 9491 (2009).
[10] M. Rochat, D. Hofstetter, M. Beck, and J. Faist, Appl. Phys. Lett. **79**, 4271 (2001).
[11] H. Luo, S. R. Laframboise, Z. R. Wasilewski, G. C. Aers, H. C. Liu, and J. C. Cao, Appl. Phys. Lett. **90**, 041112 (2007).
[12] M. A. Ordal, L. L. Long, R. J. Bell, S. E. Bell, R. R. Bell, R. W. Alexander, Jr., and C. A. Ward, Appl. Opt. **22**, 1099 (1983).
[13] E. Dupont, S. Fathololoumi, and H. C. Liu, Phys. Rev. B **81**, 205311 (2010).
[14] A. Benz, G. Fasching, A. M. Andrews, M. Martl, K. Unterrainer, T. Roch, W. Schrenk, S. Golka, and G. Strasser, Appl. Phys. Lett. **90**, 101107 (2007).
[15] P. Gellie, W. Maineult, A. Andronico, G. Leo, C. Sirtori, S. Barbieri, Y. Chassagneux, J. R. Coudevylle, R. Colombelli, S. P. Khanna, E. H. Linfield, and A. G. Davies, J. Appl. Phys. **104**, 124513 (2008).
[16] C. Walther, G. Scalari, M. I. Amanti, M. Beck, and J. Faist, Science **327**, 1495 (2010).
[17] M. Bahriz, O. Crisafulli, V. Moreau, R. Colombelli, and O. Painter, Opt. Express **15**, 5948 (2007).
[18] C. Manolatou and F. Rana, IEEE J. Quantum Electron. **44**, 435 (2008).
[19] Y. Todorov, L. Tosetto, J. Teissier, A. M. Andrews, P. Klang, R. Colombelli, I. Sagnes, G. Strasser, and C. Sirtori, Opt. Express **18**, 13886 (2010).